An amorphous nanoporous PdCuNi-S hybrid electrocatalyst for highly efficient hydrogen production

Xinxin Yang[a], Wence Xu[a], Shuo Cao[a], Shengli Zhu[a,b,c,*], Yanqin Liang[a,b,c,*], Zhenduo Cui[a,b,c], Xianjin Yang[a,b,c], Zhaoyang Li[a,b,c], Shuilin Wu[a,b,c,*], Akihisa Inoue[a,b,c,d], Luyang Chen[e]

[a] School of Materials Science and Engineering, Tianjin University, Tianjin 300072, PR China
[b] Tianjin Key Laboratory of Composite and Functional Materials, Tianjin 300072, PR China
[c] Key Laboratory of Advanced Ceramics and Machining Technology (Ministry of Education), Tianjin 300072, PR China
[d] Department of Physics, Kings Abudulaziz University, Jeddah 22254, Saudi Arabia
[e] Key Laboratory for Ultrafine Materials of Ministry of Education, School of Materials Science and Engineering, East China University of Science and Technology, Shanghai 200237, PR China

ARTICLE INFO

ABSTRACT

A novel amorphous nanoporous PdCuNi-S electrocatalyst is synthesized by a two-step dealloying method. The as-formed nanoporous PdCuNi-S catalyst exhibits excellent catalytic activity for the hydrogen evolution reaction (HER) in acidic media, which is very close to commercial Pt/C catalyst. The overpotential at 10 mA cm^{-2} and Tafel slope are 48 mV and 35 mV dec^{-1}, respectively. In addition, the catalyst shows good electrochemical stability in HER. The outstanding property of PdCuNi-S catalyst for hydrogen generation is attributed to the bicontinuous nanoporous structure, improved charge transfer, more bridging S_2^{2-} and/or apical S^{2-} in amorphous state and synergetic interactions of Pd, Cu, Ni and S.

1. Introduction

With the continuous development of economy, energy and environmental problems have become more and more serious. As a kind of affluent and clean energy source, hydrogen (H_2) is good substitute of fossil fuels to solve energy crisis and environmental pollution problems [1,2]. Highly efficient electrocatalysts are required to improve the producing of H_2. Pt-based catalysts are considered as the best catalyst for hydrogen evolution reaction (HER). However, high cost limits their applications for the industrialization [3,4]. Many efforts were carried out to design and develop highly efficient HER electrocatalysts, which were supposed to be substitute of Pt-based catalyst.

Recently, the transition metal chalcogenides have attracted many attentions due to their high efficiency for hydrogen production in acidic media. Some pure metallic atoms were introduced into the transition metal chalcogenides to take up the structural edges and increase the activity sites [5]. Among all the researches about the transition metal chalcogenides, MoS_2-based compounds is the most fascinating [6]. Low onset overpotential for HER was obtained in defect-rich MoS_2 ultrathin nanosheets and amorphous MoS_2 films [7]. However, the relatively low conductivity and unstability in long-term HER testing are still important problems for most MoS_2 catalysts [8].

Palladium, owing to similar chemical property with Pt and lower cost than Pt, has been considered as a good substitute of Pt for hydrogen-related catalytic applications [9]. The nanoporous Pd (np-Pd) catalyst could be prepared by dealloying method [10]. The properties of Pd-based nanocatalysts are influenced by morphology [11], particle size [12] and structure [13]. However, strong Pd-H bonding hinders the H_{ads} desorption in catalytic processes [14]. Some attempts were carried out to improve its catalytic performance [15]. In our previous work, we found that palladium sulfide (Pd-S) exhibited better catalytic properties than nanoporous palladium (np-Pd) due to more active sites which were provided by S [16]. In addition, relative higher solid solubility of H in Pd would lead to the lattice expansion, furthermore form hydride phases which would decrease long-term stability [17]. The introduction of some metallic atoms, such as Ni, Cu, and Co, could suppress the formation of hydride [18]. Moreover, the introduction of these metallic atoms could improve the electrocatalytic performance due to the electronic effect [19]. Furthermore, these metallic atoms not only could provide additional active sites and improve the electron transfer rate, but also facilitate the adsorption of the atomic hydrogen produced and its subsequent association to form H_2 from these intermediates [20].

In the present work, a new multicomponent nanoporous PdCuNi-S catalyst was synthesized through a two-step dealloying method. The as-

prepared PdCuNi-S catalyst exhibits excellent catalytic activity and long-term stability for HER, which is very similar with Pt catalyst in acidic media. The price is relative cheaper than commercial Pt catalyst. This multicomponent nanoporous PdCuNi-S catalyst would be an appropriate substitute for Pt catalyst in HER.

2. Materials and methods

2.1. Experimental section

The master alloy with composition of $Al_{80}Pd_{10}Cu_5Ni_5$ (at. %) was prepared by arc melting the mixture of pure Pd, Cu, Ni and Al metals in Ti-gettered high-purity argon atmosphere. $Al_{80}Pd_{10}Cu_5Ni_5$ ribbon was prepared using melt-spinning method [16,21–24]. The master alloy was remelted in quartz tubes and ejected onto a Cu wheel rotating for rapid solidification to form the alloy ribbons. These ribbons were typically 30–50 μm in thickness, 2–4 mm in width. The $Al_{80}Pd_{10}Cu_5Ni_5$ ribbon was dealloyed in the 1.0 M KOH solution at room temperature to obtain PdCuNi intermediate. Subsequently, the nanoporous PdCuNi-S catalyst was obtained by further immersing the PdCuNi intermediate in 15 M H_2SO_4 solution at 363 K for 48 h. The reaction mechanism between concentrated H_2SO_4 and PdCuNi intermediate is still not clear but we think the formation mechanism is similar to CuS in our previous work [23]. The reaction process can be summarized as follows:

$$2Al + 2KOH + 2H_2O \rightarrow 2KAlO_2 + 3H_2 \tag{1}$$

$$M + H_2SO_4 \rightarrow MSO_4 + M_xS_y + SO_2 + H_2O \ (M: Cu, Ni, Al) \tag{2}$$
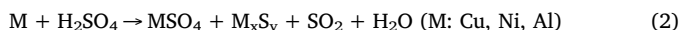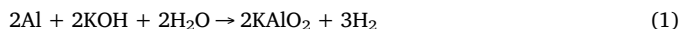
The valence of S gradually evolves from −1 to −2 and S content increase gradually in chemometrics [16]. The formation of palladium sulfide is easier than copper sulfide and nickel sulfide because of the solubility product constant of palladium sulfide 2.03×10^{-58}) is much lower than that of copper sulfide (6.3×10^{-36}) and Nickel sulfide (1.4×10^{-27}). For comparison, nanoporous Pd-S, PdCu-S and PdNi-S were prepared by dealloying $Pd_{20}Al_{80}$, $Al_{80}(Pd_{0.67}Cu_{0.33})_{20}$ and $Al_{80}(Pd_{0.67}Ni_{0.33})_{20}$ ribbons using same processes, respectively. Finally, all the samples were rinsed in distilled water and ethyl alcohol for several times and dried at 303 k for 24 h in a vacuum drying oven.

2.2. Materials characterization

The morphologies of as-prepared catalysts were examined by scanning electron microscope (SEM, Hitachi S-4800) and transmission electron microscope (TEM, JEOL2100 M). X-ray diffraction (XRD, Bruker D8) and X-ray photoelectron spectroscopy (XPS, PHL 1600ESCA) were used to analyze the phase and surface chemical state, respectively. The specific surface area and the pore size distribution were determined using the Brunauer-Emmett-Teller (BET) method and the Barrett-Joyner-Halenda (BJH) method by an autosorb iQ instrument (Quantachrome). H_2 temperature programmed reduction (H_2-TPR) profiles of the calcined catalysts were recorded using an Auto Chem II 2920 apparatus. 50 mg of sample was placed in a quartz reactor and heated at 10 °C/min up to 300 °C under a He flow of 50 ml/min, and heated at this temperature for 2 h. Then the reactor was cooled down to 50 °C. H_2-TPR was performed using a 10% H_2/Ar mixture at a flow rate of 50 ml/min while the temperature was linearly ramped from 50 °C to 800 °C at 10 °C/min.

2.3. Electrocatalytic measurements

The electrochemical tests were conducted using a Gamry interface 1000 electrochemical workstation with a conventional three-electrode electrochemical system. A carbon rod and a saturated calomel electrode (SCE) served as the counter and reference electrodes, respectively. The working electrodes were prepared as following process: The 4 mg catalyst was dispersed in a mixed solution containing 900 μl isopropyl

alcohol and 100 μl 5% Nafion solution. The sonication was applied to make the suspension homogeneous. Then 100 μl catalyst ink was coated onto the glassy carbon (GC) electrode (6 mm in diameter) and then dried at room temperature. Commercial Pt/C catalyst (20 wt%, Alfa Aesar) was used as a control group. Linear sweep voltammetry (LSV) was performed in nitrogen-saturated 0.5 M H_2SO_4 at the scan rate of 2 mV s^{-1}. Cyclic voltammetry (CV) was carried out with various scan rates between 0.24 and 0.34 V vs. RHE to estimate the electrochemical active surface area (EASA). The electrochemical impedance spectroscopy (EIS) was measured with frequencies ranging from 10^{-2} Hz to 10^5 Hz. The long-term stability was tested under static overpotential of 200 mV for 24 h. In addition, 5000 cycles LSV was also performed in 0.5 M H_2SO_4 at the scan rate of 50 mV s^{-1}. The potential was converted to the reversible hydrogen electrode (RHE) according to the following equation:

$$E_{RHE} = 0.059*pH + 0.241 + E_{SCE} \tag{1}$$

In addition, the equations of iR_s- compensated, the Exchange current density (j_o) and the turnover frequencies (TOF) are the same with our previous work [16].

3. Results and discussion

3.1. Morphology and structure of catalysts

The synthetic procedure diagram of two step dealloying is shown in the Fig. 1. Fig. 2a shows the SEM images of PdCuNi sample which was subjected to first-step dealloying. This sample consist of some rods with hundreds nanometers in length and tens nanometers in diameter. No obvious bicontinuous nanostructure could be observed in the sample. After the second-step dealloying, the morphology of the sample PdCuNi-S is distinctly different from the PdCuNi sample. A nanoporous structure was formed on the nanorods (as shown in Fig. 2b). TEM image (Fig. 2c) indicates that the PdCuNi-S sample would have a typical bicontinuous nanoporous structure with the interconnected ligaments and pore diameter of about 10 nm. The high-resolution transmission electron microscopy (HRTEM) image of PdCuNi-S catalyst is shown in Fig. 2d. The absence of lattice fringes and selective area electron diffraction (SAED) pattern indicate the amorphous nature. The elemental mapping of Pd, Cu, Ni and S from a selected area is shown in Fig. S1. These elements distribute homogeneously. The N_2 adsorption-desorption isotherms (as shown in Fig. S2) show that the surface area of PdCuNi-S is 27.229 m^2 g^{-1} and the average pore diameter is 9.86 nm, which is consistent with the SEM and TEM images.

The X-ray diffraction (XRD) pattern of the precursor alloy and the corresponding dealloyed samples are shown in Fig. 3a. The α-Al and Al_3Pd phases are identified in original AlPdCuNi ribbon. There are no obvious peaks concerned with Cu and Ni, indicating the doping of Cu and Ni in α-Al based phases. After dealloying, the XRD patterns of as-prepared PdCuNi and PdCuNi-S show only broad halos, suggesting the amorphous transition during dealloying process. Fig. S4 and Table S1 show the EDX spectra and compositions of the $Al_{80}Pd_{10}Cu_5Ni_5$ ribbon and as-dealloyed samples, respectively. It can be seen that there is still a small amount of Al atoms in the sample after two step dealloying, indicating that the Al could not be removed completely under the present conditions. In some similar nanoporous materials, it is considered that the residual Al has no effect on the catalytic performance of the surface [21,25]. During the first dealloying step, the main reaction is that dissolution of the α-Al phase into KOH solution, which would produce large channels. These large channels is favor in the later sulfurization process. During the second dealloying in the sulfuric acid, the element of S is introduced into the PdCuNi sample. Meanwhile, Al, Cu and Ni atoms are further removed and lots of smaller nanopores are formed. In this step, the H_2SO_4 solution serves as not only reactant, but also sulfur source [26,27]. Dealloying mechanism could be described as : because
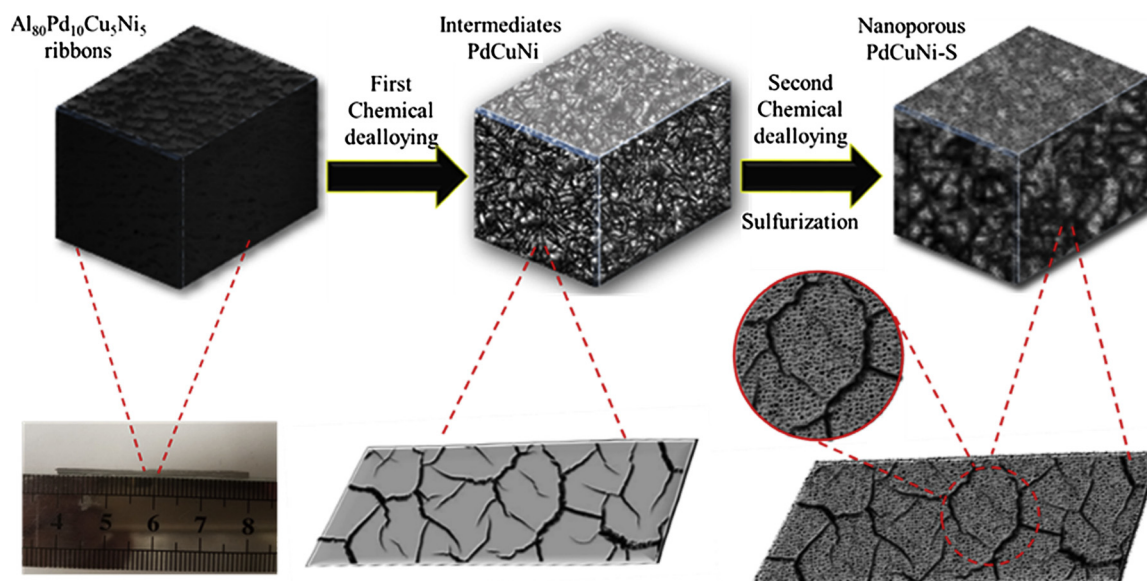
Fig. 1. Synthetic procedure for nanoporous PdCuNi-S catalyst: two step dealloy method.

Pd atom in the catalyst is more stable than Al、Cu and Ni atoms in concentrated H_2SO_4 solution, which leads to Al、Cu and Ni atoms dissolved into the solution and the rest of Pd, Cu and Ni elements re-arranged and gathered into the ligament-channel nanoporous structure via spinodal-decomposition [11]. This structure is like a core-shell consisting of a Pd-rich shell surrounding a Pd-Cu or Pd-Ni core [16].

The SEM images of PdCu-S、PdNi-S and Pd-S catalysts (control samples) are also shown in Fig. S3. All samples exhibit the similar bi-continuous nanostructures. In addition, the N_2 adsorption-desorption isotherms (as shown in Fig. S2) show that the specific surface area of PdCuNi-S ($27.229\,m^2\,g^{-1}$) is higher than that PdCu-S ($23.681\,m^2\,g^{-1}$), PdNi-S ($20.007\,m^2\,g^{-1}$) and Pd-S ($20.298\,m^2\,g^{-1}$). The Fig. 3b shows the XRD results of PdCu-S, PdNi-S and Pd-S catalysts. The Pd phase is identified in PdNi-S and Pd-S catalysts and the Pd_4S phase is identified in PdCu-S sample. The relative broad diffraction peaks would mainly result from the large surface stress generated during dealloying process, since the grain size of the alloy samples is on the order of few micro-meters [28]. It is worth to notice that the PdCu-S, PdNi-S and Pd-S are not amorphous, which is different with the PdCuNi-S. The amorphous phase is a kind of non-equilibrium state. In general, the fabrication with high energy probably transform the solid crystal phase to the solid amorphous phase, such as diffusion reaction [29], ion irradiation [30] and mechanical alloying [31]. Another possibility is that free energy of original crystal phase would be higher than that of the amorphous phase [32]. In our case, the formation of amorphous PdCuNi-S is under a relatively low temperature, which indicating the absence of high
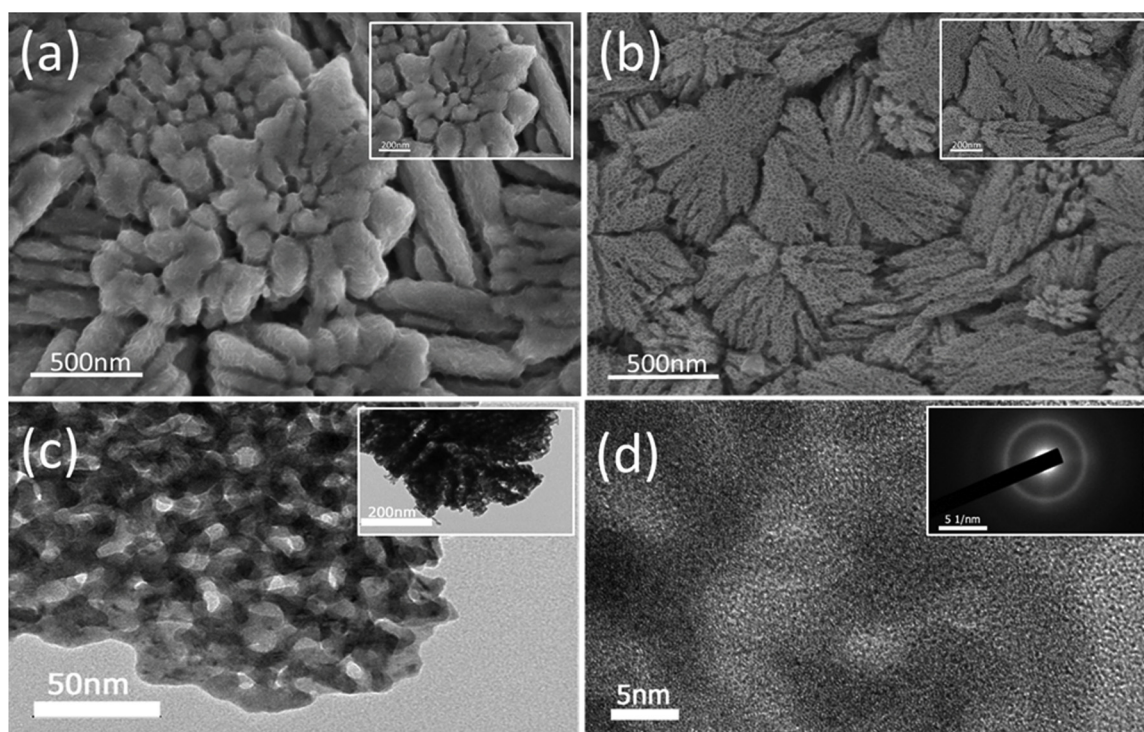

Fig. 2. SEM images of as-prepared PdCuNi (a) and PdCuNi-S (b). TEM (c) and HR-TEM (d) images of PdCuNi-S catalyst.
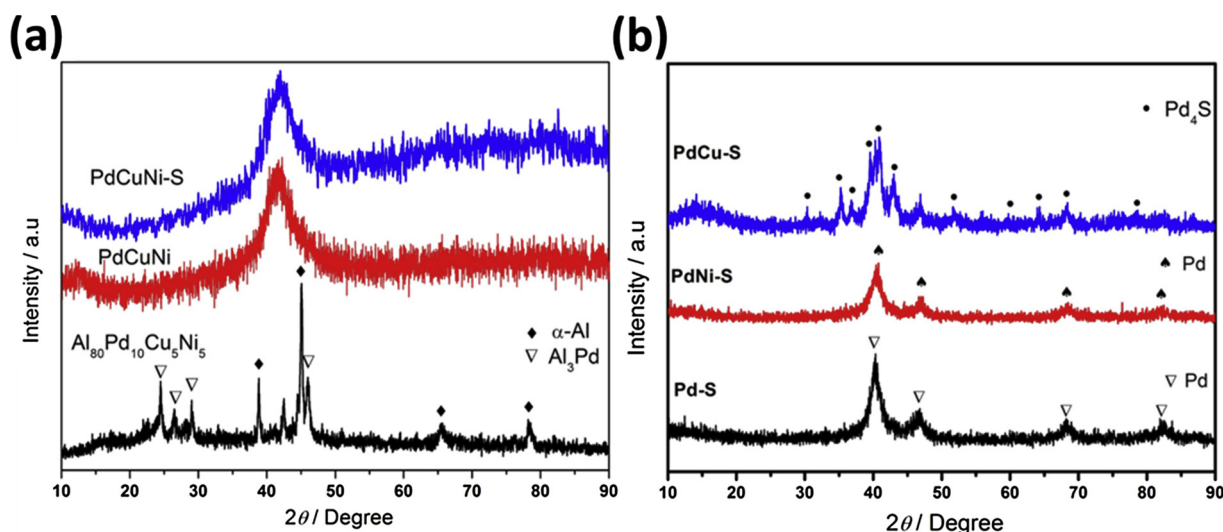
Fig. 3. (a) XRD patterns of $Al_{80}Pd_{10}Cu_5Ni_5$, PdCuNi and PdCuNi-S samples and (b) XRD patterns of PdCu-S, PdNi-S and Pd-S samples.

energy during the dealloying process. The driving force of amorphisation should be high free energy of original crystal phase. Since the original alloy ribbon was prepared by melt-spinning method (a kind of rapid cooling method), it should be in another non-equilibrium state. It was reported that some crystal states obtained under rapid cooling condition would have higher free energy than the amorphous state [33]. Moreover, compared with other elements (Al, Cu and Ni), the diffusion coefficient of Pd is much lower. As a result, other elements diffusion and rearrangement are restrained [34]. The serious difference of diffusion coefficient between Pd and other elements would favor in the formation of amorphous phase [35]. According to the classical empirical rules, multi-components, large difference of atom size and negative mixing enthalpy are benefit in the formation of amorphous alloy [36]. The as-formd PdCuNi or PdCuNi-S are compose of 4 kinds of metallic elements (Pd, Cu, Ni and small amount of Al). There are sufficient atom size difference (the atomic radius of Pd, Cu, Ni and Al are 0.137 nm, 0.128 nm, 0.124 nm and 0.143 nm, respectively). The mixing enthalpies of main atom pairs are negative (the mixing enthalpies of Pd-Cu, Pd-Ni and Pd-Al are −14, 0 and −46 kJ mol^{-1}, respectively) [37]. Hence the PdCuNi or PdCuNi-S could be easy to form amorphous phase. However, the amorphization during the dealloying is rather complex since there is not only atom diffusion and rearrangement, but also removal of active atoms. More in-depth investigation will be carried out in the future's work. Compared with the crystal phase, amorphous phase could offer more diversity and flexibility of composition and microstructure since their surface chemistry could be adjusted on the molecular level [38]. The amorphous phase provides high concentration of active sites and nanoporous structure is favor of the electrolyte diffusion during the HER process [39].

XPS spectra of the PdCuNi-S catalyst are shown in Figs. 4 and S5. The full profile demonstrates the presence of Pd, Cu, Ni and S. The Pd 3d spectrum is fitted to two doublets. Two characteristic peaks located at 342.5 eV and 337.3 eV can be assigned to Pd^{2+} and the peaks located at 341.6 eV and 336.2 eV can be attributed to Pd°, respectively [40]. The main peak at 932.5 eV and the sub-peak at 952.7 eV are corresponding to Cu $2p_{3/2}$ and Cu $2p_{1/2}$ of Cu^+ [24], respectively. Two Ni 2p peaks locate at 854.9 eV and 853.2 eV, which can be indexed as the Ni^{2+}. The additional doublet peaks at 862.6 eV and 857.4 eV are related with the shakeup satellite peaks [41]. The peak of XPS is relatively chaotic due to the relatively low nickel content on the final surface. The spectra of S 2p can be divided into six peaks. The higher bridging energies of S $2p_{1/2}$ and S $2p_{3/2}$ at 165.0 eV and 165.8 eV are corresponding to bridging S_2^{2-} and/or apical S^{2-} [42,43]. Meanwhile, the lower peaks locate at 163.94 eV and 163.8 eV, suggesting the existence

of terminal S_2^{2-} and/or S^{2-} in the catalyst [42]. The rest of binding energy at 168.9 eV and 170.0 eV in S 2p spectrum is due to SO_4^{2-} incorporated into the material which was formed in the second dealloying process [43,44]. According to some researches, the exist of higher binding energy bridging S_2^{2-} and/or apical S^{2-} in the catalyst surface could improve the catalytic performance [42].

The results of H_2-TPR are shown in Fig. S6. All Pd-based catalysts showed a negative H_2 consumption peak under 100 °C, attributed to the decomposition of β-palladium hydride (β-PdH$_x$) which was formed from the adsorption of hydrogen within the structure of metallic Pd° at room temperature [45]. In the case of Pd-S catalyst, another H_2 consumption peak was observed in the temperature of 425 °C. In addition, there is a peak at about the same temperature on the other three catalysts, which was called peak II. Peak II could be attributed to the reduction of Pd^{2+} to Pd. Compared with the catalysts PdCuNi-S and PdCu-S, peak I might be assigned to the reduction of Cu^+ to Cu [45]. As for the peak III, it could be thought of as the process of Ni^{2+} being reduced by comparing the catalysts PdCuNi-S and PdNi-S. The test results of H_2-TPR is basically consistent with that of XPS.

3.2. Electrochemical hydrogen evolution performance

Polarization measurement was first proceeded to evaluate the optimal mass loading of the catalysts. As shown in Fig. S6, the appropriate loading amount is 1.42 mg cm^{-2}. Fig. 5a shows the LSV curves of as-prepared catalysts. The detailed information for HER performance of PdCuNi-S, PdCu-S, PdNi-S, Pd-S and PdCuNi are list in Table 1.The PdCuNi exhibits the lowest catalytic activity, suggesting the sulfurization process would effectively modify the activity. It is obvious that the PdCuNi-S catalyst requires quite small overpotential of 48 mV (for the current density of 10 mA cm^{-2}), which is much lower than that of PdCuNi (161 mV), Pd-S (149 mV), PdNi-S (103 mV), PdCu-S (73 mV) and close to that of commercial Pt/C (36 mV). The PdCuNi-S exhibits predominant catalytic activity compared to the other HER catalysts reported previously (as summarized in Table S2). Moreover, the PdCuNi-S catalyst displays a large cathodic current density of 106.3 mA cm^{-2} at an overpotential of 100 mV, which is equivalent to 76.6 A g^{-1} by normalization with the loading Pd mass. That is 3.6 and 5.5 times higher than that of the nanoporous PdCu-S and PdNi-S catalysts, respectively (Fig. S8). According to LSV test results, the hydrogenation properties of PdCu-S and PdNi-S are higher than that of Pd-S, which indicated that the addition of Cu and Ni could promote the hydrogen analysis of catalyst. Moreover, the amorphous nanoporous PdCuNi-S exhibits remarkable activity in comparison with the other samples. In
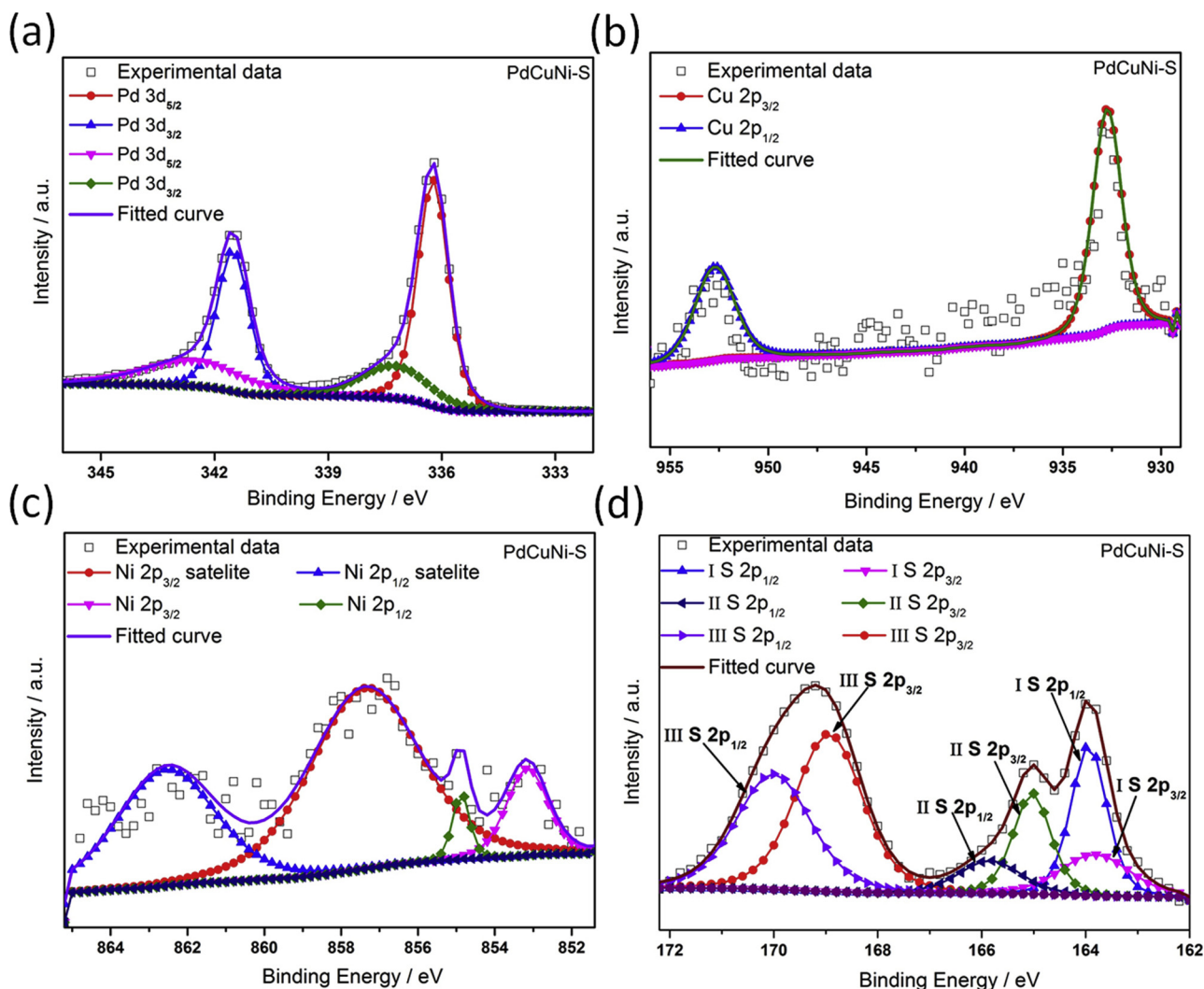
Fig. 4. Detail XPS of Pd 3d (a), Cu 2p (b), Ni 2p (c) and S 2p (d) of PdCuNi-S catalyst.

addition, it can be seen that co-addition of Cu and Ni is more advantageous to form amorphous structure. The amorphous structure means homogeneous surface and lack of the long-range, which could provide more defect sites to act as active centers during the HER process [38,46]. Furthermore, it confirms that the addition of Cu or Ni in the precursor alloy can have a impact on the activity of the material and the incorporation of Cu and Ni accounts for the best electrocatalytic activity. According to some previous reports, the existence of Cu atoms favors to reduce the obstruction of H_{ads} formation [20,47]. In addition, the Ni edges not only boost the decomposition of H_2O, but also make for the production of H_{ads} [20,48].

To figure out the response kinetics of the catalysts, Tafel plots of PdCuNi-S, PdCu-S, PdNi-S, Pd-S, PdCuNi and Pt/C are presented in Fig. 5b. The commercial Pt/C catalyst shows a lowest Tafel slope of 31 mV dec^{-1}, which is consistent with previously report [49]. The amorphous nanoporous PdCuNi-S shows a slope of 35 mV dec^{-1}, much lower than that of PdCu-S (56 mV dec^{-1}), PdNi-S (80 mV dec^{-1}), Pd-S (102 mV dec^{-1}) and PdCuNi (118 mV dec^{-1}). A smaller Tafel slope implies that the HER rate of the PdCuNi-S would increase more rapid with increasing overpotential [50]. There are three main reactions steps involved in the HER, which are the electrochemical hydrogen adsorption (Volmer), electrochemical desorption (Heyrovsky) and chemical desorption (Tafel) reactions [51]. Tafel slopes of about 30, 40 and 120 mV per decade mean that the rate-determining step are Tafel, Heyrovsky, and Volmer reaction, respectively [15]. The Tafel slope of

35 mV dec^{-1} for the PdCuNi-S catalyst indicates the Volmer-Tafel mechanism [52]. The exchange current density (j_0) is another vital kinetic parameter which represents the electron migration. The exchange current density was measured by employing the extrapolation method [53]. From Table 1, it can be seen that j_0 of PdCuNi-S catalyst is much higher than that of other catalysts, indicating its remarkable electron migration ability.

In order to evaluate the amount of active sites, electrochemical active surface area (EASA) is measured via a series of double-layer charging currents at different scan rates [24] (as shown in Figs. S9 and S10). The EASA of PdCuNi-S catalyst is obviously higher than that of PdCuNi catalyst. It is more likely that the enhanced activity should result from the doping of S active sites, which are generated on the surface of the amorphous phase [54]. At the same time, the capacitance value of both PdCu-S and PdNi-S are much lower than that of the PdCuNi-S catalyst (shown in Fig. S9), which indicates the co-addition of Cu and Ni would have better improvement effect on the electrocatalytic activity. The turnover frequencies (TOF) values are calculated to compare the intrinsic catalytic activity of each catalyst (as shown in Fig. 5d). The TOF value of the PdCuNi-S catalyst is 0.032 s^{-1} at overpotential of 100 mV, which is about 3.6, 4.98, 28.98 and 106.3 times higher than that of PdCu-S, PdNi-S, Pd-S and PdCuNi catalysts, respectively. The results of TOF are consistent with the previous LSV results. Since the nature of the active sites of the catalyst is not clearly understood yet, the TOF of the as-prepared materials were calculated
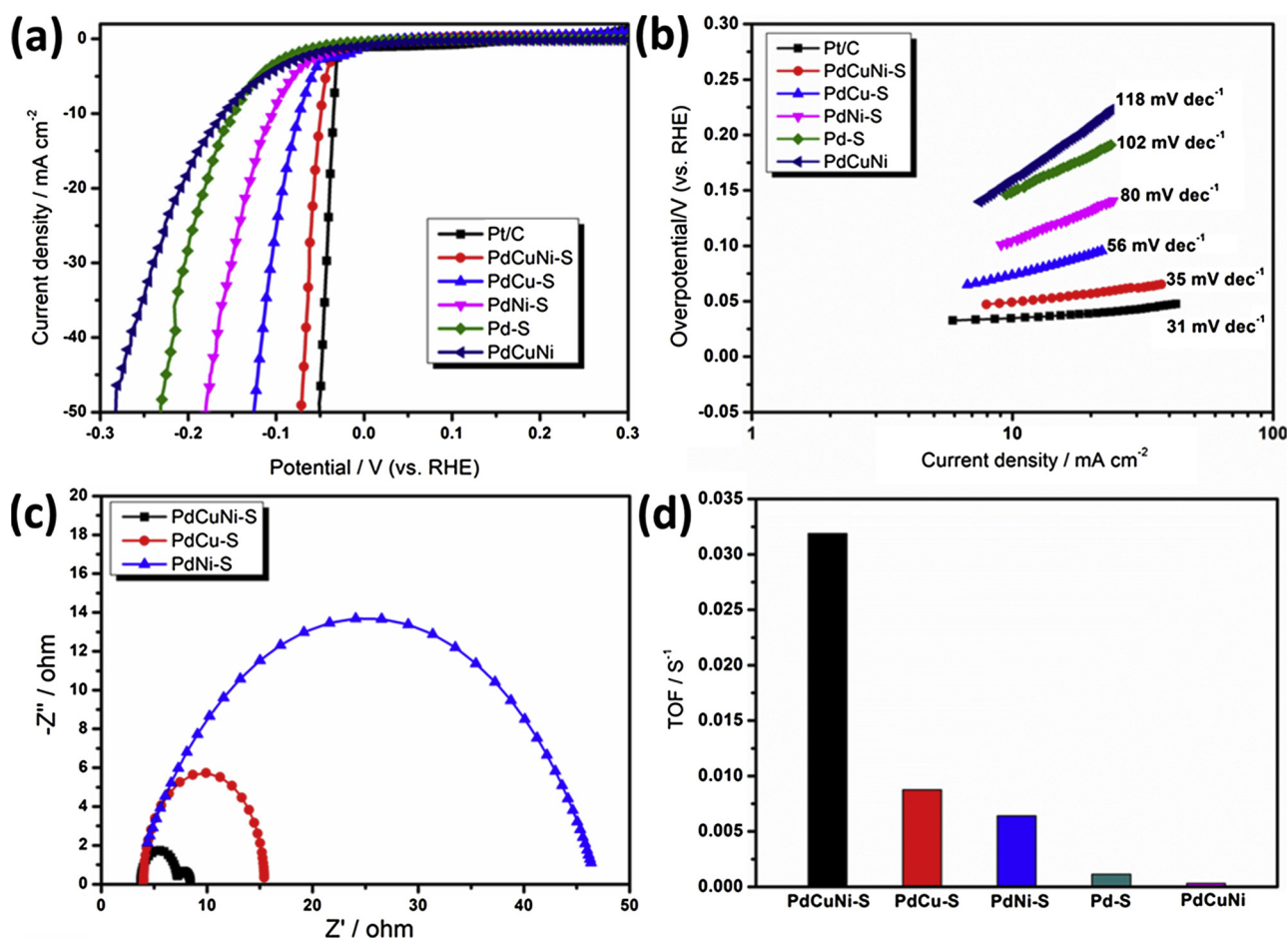
Fig. 5. (a) LSV polarization curves of PdCuNi-S, PdCuNi, Pd-S, PdCu-S, PdNi-S and Pt/C in 0.5 M H_2SO_4 with a scan rate of 2 mV s^{-1}. (b) The corresponding Tafel plots of PdCuNi-S, PdCuNi, Pd-S, PdCu-S, PdNi-S and Pt/C. (c) EIS spectra of PdCuNi-S, PdCu-S and PdNi-S at 100 mV overpotentials. (d) Calculated TOF values of the as-prepared Pd-based materials.

Table 1
Comparison of catalytic parameters of different catalysts in 0.5 M H_2SO_4 solution.

catalyst	overpotential at 10 mA cm^{-2} (η_{10})	overpotential at 50 mA cm^{-2} (η_{50})	Tafel slope (mV dec^{-1})	TOF (s^{-1})	j_0 (μA cm^{-2})
PdCuNi-S	48	71	35	0.03188	385.45
PdCu-S	73	125	56	0.0088	312.29
PdNi-S	103	181	80	0.0064	286.36
Pd-S	149	232	102	0.0011	265.63
PdCuNi	161	283	118	0.0003	186.53

by the amount of substance rather than the amount of active sites. Therefore the TOF values of all the catalysts might be underestimated in this paper [16,24]. In conclusion, the introduction of Cu、Ni and S not only increased the number of electrochemical active sites, but also enhanced the intrinsic catalytic activity of catalysts.

Electrochemical impedance spectra (EIS) was applied to get insight into the catalytic kinetic. Fig. 5c and Fig. S11a show the Nyquist plots of PdCuNi-S, PdCu-S, PdNi-S, Pd-S and PdCuNi at the overpotential of 100 mV. The promoted hydrogen evolution efficiency of as-prepared PdCuNi-S can be explained by the reduced charge-transfer resistance. The Nyquist plots of PdCuNi-S material can be fitted as an equivalent circuit model-1 (shown in Fig. S12a). R_s, R_1 and R_{ct} represent the resistances of the electrolyte, electrode porosity and charge-transfer, respectively [55]. In this model, the high frequency semicicle (CPE$_1$-R$_1$) is

related to the porosity of the electrode and the low frequency semicicle (CPE$_2$-R$_{ct}$) is related to the kinetics of the faradaic reaction of the HER [55,56]. The R_{ct} value of PdCuNi-S catalyst decreases with increasing overpotentials (Fig. S11b and Table S3). Lower value of R_{ct} means faster catalytic rate at higher overpotentials [57]. Another equivalent circuit model-2 (shown in Fig. S12b) was appiled to fit other control Pd-based metarial. As the same with model-1, R_s represent the resistances of the electrolyte and CPE- R_{ct} is related to the kinetics of the HER process [47,56]. Since R_{ct} has a strong relationship with the HER catalytic activity, Table S4 summarizes the fitting parameters of PdCuNi-S, PdCu-S, PdNi-S, PdCuNi and Pd-S catalyst at overpotential of 100 mV. The PdCuNi-S (1.263 Ω) exhibits the smallest R_{ct} value among all the catalysts, which imply the fastest charge transfer process during the process of hydrogen production. The R_{ct} value of the catalyst after sulfuration is much lower than PdCuNi (127.9 Ω), which indicates that the incorporation of S would be beneficial to improve charge transfer process. In addition, the R_{ct} value of the PdCu-S (11.46 Ω) or PdNi-S (43.73 Ω) samples is lower than that of Pd-S (137.7 Ω). This implies that the introduction of Cu or Ni could also improve the charge transfer process. Furthermore, the co-addition of Cu and Ni could also increase the rate of charge transfer process since PdCuNi-S has smallest R_{ct}. The superior activity of PdCuNi-S is closely interrelated with its surface morphology and surface electronic structure. The typical bincontinuous nanoporous structure enhances the specific surface area, and in turn promotes the transmission of proton and conduction of electrons. The amorphous structure provides more active sites to improve the proton and charge exchange efficiency [38,46]. The introduction of Cu、Ni and S improve the intrinsic catalytic activity and the synergistic effect
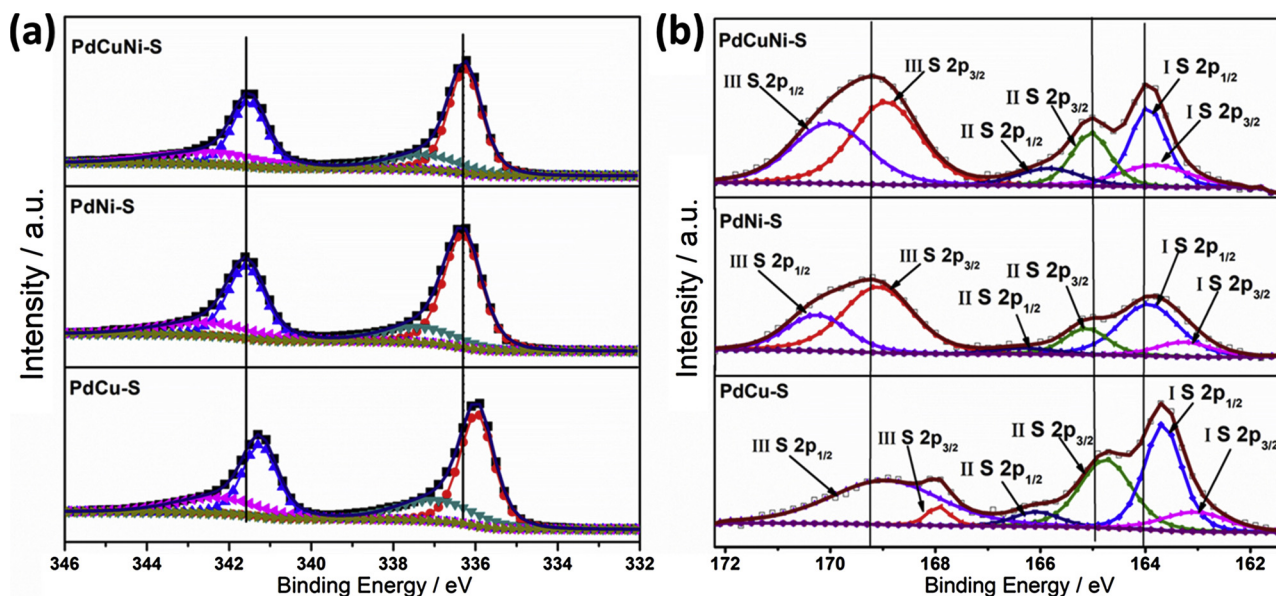
Fig. 6. (a) Pd 3d spectra of the as-prepared PdCuNi-S、PdNi-S and PdCu-S catalysts, (b) S 2p spectra of the as-prepared PdCuNi-S、PdNi-S and PdCu-S catalysts.

among these atoms also accelerate the charge transfer process and the proton adsorption process.

The surface composition and structure of the catalyst has great influence on the catalytic performance [14]. The S and Pd in PdCuNi-S catalyst would play a significant role in the catalytic performance. In addition, the presence of Cu and Ni could modify the electronic structure of S and Pd. To get further insight the synergistic effect of Cu、Ni、Pd and S on the catalytic mechanism, XPS of Pd and S in the PdCuNi-S, PdCu-S and PdNi-S catalysts are shown in Fig. 6. Compared to the PdCu-S catalyst, the Pd 3d peaks of the PdCuNi-S and PdNi-S catalyst shifts to higher values (as shown in Fig. 6a), indicating depletion of d valence electron charge at a Pd site since the binding energy shift depends on the charge redistribution of a valence electron [16,58,59]. In some reports about Molybdenum sulfide materials [16,38], the number of S, especially the higher binding energy of bridging S_2^{2-} and/or apical S^{2-}, exhibits enhanced the activity of hydrogen evolution [44]. Louisa's team found that the bridging S_2^{2-} sites would be of a similar motif to the MoS_2 slab edge sites with a moderately positive hydrogen binding energy through calculating the S−H binding strengths. This implies that these S_2^{2-} could be the most active sites in the amorphous metal sulfide system [44]. The S 2p XPS spectra are shown in Fig. 6b, which II S peak is the higher binding energy of bridging S_2^{2-} and/or apical S^{2-} and I S peak is the terminal S_2^{2-} and/or S^{2-}. By comparing the ratios of these two S atoms, the PdCuNi-S and PdCu-S have the similar intensity ratio of II S/I S (about 0.71 and 0.80, respectively). The intensity ratio of II S/I S of PdNi-S is 0.39, which imply that the existence of Cu would be favor in the generation of the higher binding energy of S atoms. In addition, the II S $2p_{3/2}$ and I S $2p_{1/2}$ peaks of the PdCuNi-S and PdNi-S catalysts shifts to higher values than the PdCu-S catalyst. Furthermore, the surface S/Pd atomic ratio of all catalysts are shown in Fig. S13 and Table S5. The Pd-S catalyst has the smallest S/Pd ratio about 1:5. The PdNi-S and PdCu-S have the similar S/Pd ratio about 1:3. While the PdCuNi-S catalyst has the highest S/Pd ratio about 1:2. This indicates that the coexist of Cu and Ni would be beneficial to increase the ratio of S/Pd in the surface of catalysts. The PdCuNi-S exhibit a higher binding energy of Pd 3d and S 2p peaks and more bridging S_2^{2-} and/or apical S^{2-} active sites in the surface, therefore, displaying outstanding HER activity. In addition, we also compared the XPS of Cu 2p and Ni 2p in the PdCuNi-S, PdCu-S and PdNi-S catalysts (shown in Fig. S14). The peak of Cu 2p and Ni 2p also shifts positively for PdCuNi-S catalyst as the same with the result of Pd 3d, which indicating the improvement of electronic structure for both

Pd, Cu and Ni atoms. It has been previously reported that the bond strength can be effectively improved by alloying the left-hand side transition metals with the right-half transition metals, thus the intermetallic stability is increased, which is consistent with d-electrons for the synergism and catalytic activity [16,58,59]. The electron transfer from Pd to Cu and Ni atoms leads to a synergistic effect, which decreases the hydrogen binding energy and benefits the desorption of H_{ads} and subsequent H_2 formation [16,59,60]. As we all know, the HER activity is determined by the hydrogen absorption energy [50] and the hydrogen absorption energy is influenced by the intrinsic activity of each active site [50]. According to above analysis, Pd alloyed with Cu and Ni could change the intrinsic activity of each active site, which further gains the balance between the amount of active sites and the improved intrinsic activity of the active sites, resulting in the best hydrogen evolution performance.

Excellent catalysts also require long-term stability for practical application [61]. The potentialstatic curve for PdCuNi-S at an overpotential of 200 mV is shown in Fig. 7a. The curve shows a typical sawtoothed shape, which is due to the accumulation and release of the bubbles [16]. Even after 24 h, the reaction remains stable, indicating excellent stability. The recycling CV measurement for the PdCuNi-S catalyst was also carried out. As shown in Fig. 7b, after 5000 cycles, the CV curve of the PdCuNi-S exhibits only slight deviation from the initial curve. The XPS results of PdCuNi-S after 5000 cycles CV test are showed in the Fig. S16. The Pd 3d peaks shift to lower values and the higher binding energy peaks of S still remain. However, the ratio of II S/I S decreases to 0.35, indicating that some bridging S_2^{2-} and/or apical S^{2-} would transform to terminal S_2^{2-} and/or S^{2-}. The TEM and HRTEM images (Fig. S15) demonstrate that amorphous structure, nanoporous morphology and the uniform distribution of PdCuNi-S have no significant change after 5000 CV cycles.

3.3. Hydrogen evolution catalysis mechanism and reasons

On the basis of above results, it can be found that amorphous nanoporous PdCuNi-S catalyst has the best hydrogen evolution performance among all materials. In order to clearly investigate the reasons for the improvement of hydrogen evolution catalytic performance of PdCuNi-S catalyst, the catalytic mechanism would be discussed from the following aspects in combination with schematic diagram (shown in Fig. 8) and the previous test results. (1). According to the test results of BET (shown in Fig. S2) and cyclic voltammetry (shown in Figs. S9 and
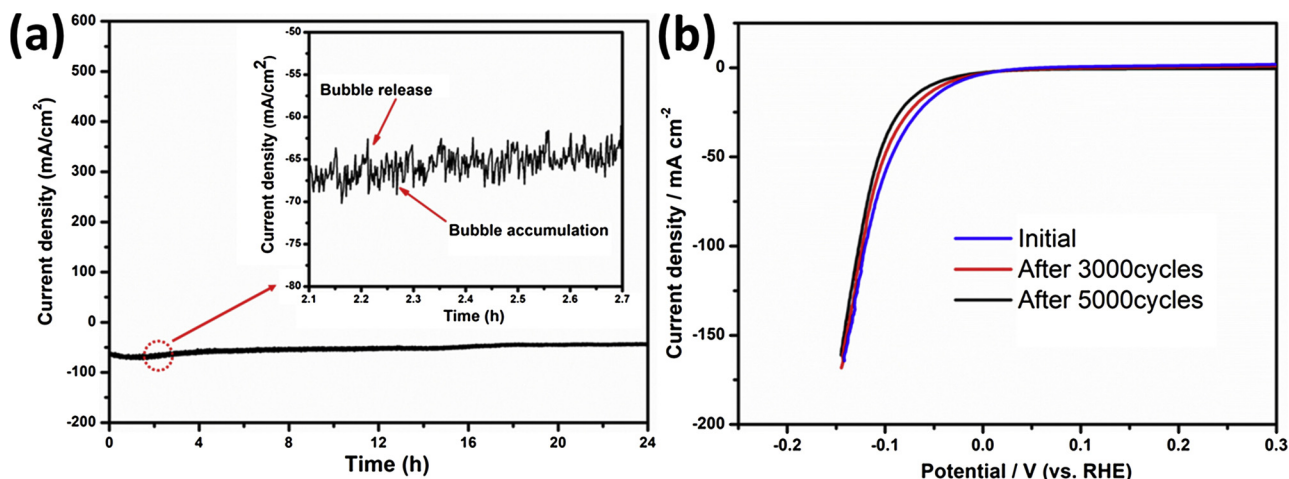
Fig. 7. (a) Stability tests of the PdCuNi-S catalyst under static overpotential of 200 mV in 0.5 M H_2SO_4 and (b) Durability test of PdCuNi-S catalyst before and after 5000 cycles in 0.5 M H_2SO_4.
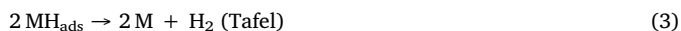
S10), the catalyst PdCuNi-S has the highest specific surface area and electrochemical surface area, indicating that PdCuNi-S catalyst exposes the most active sites which exhibits the best HER activity. In addition, the nanoporous structure (10 nm in Fig. 2b and Fig. S2) is not just beneficial for the diffusion and adsorption of H^+ ions on the whole PdCuNi-S catalyst, but also to the rapid capture of electrons by adsorbed H^+ ions owing to the short transportation route. (2). According to previous research [46], in acidic systems, the possible mechanism of hydrogen evolution is as follows: The first step is the electrochemical hydrogen adsorption step.

$$H_3O^+ + e^- + M \rightarrow MH_{ads} + H_2O \text{ (Volmer)} \quad (1)$$
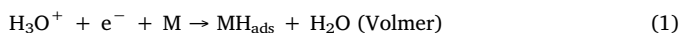
The Volmer step is followed by either the electrochemical desorption step

$$MH_{ads} + e^- + H^+ \rightarrow M + H_2 \text{ (Heyrovsky)} \quad (2)$$

Or the chemical desorption step

$$2 MH_{ads} \rightarrow 2 M + H_2 \text{ (Tafel)} \quad (3)$$

Based on the results of the Tafel slope (Fig. 5b), which is an intrinsic feature for electrocatalysts, the PdCuNi-S catalyst is the smallest among all the samples. And according to the TOF (Fig. 5d) and EIS (Fig. 5c and Fig. S11) results, almost all the samples conform to the same rules, which consistent with the tafel slope. It could be the co-addition of Cu and Ni improves the electronic structure and composition of the catalyst surface, which decrease the hydrogen binding energy and in turn benefited the desorption of H_{ads} and H_2 formation, resulting in the best hydrogen evolution performance. According to the above XPS analysis (Fig. 6), in order to explain the differences of different catalysts more clearly, a possible electrocatalytic hydrogen evolution mechanism was proposed, as shown in Fig. 8, compared with the catalyst Pd-S (Fig.8A), the addition of Ni (Fig.8B) or Cu (Fig.8C) atoms is not only the active site itself, but also changes the electron structure of the Pd atoms around and the composition of surface. Our previous work [16] confirmed that Cu could easily obtain electrons from neighboring Pd atoms, which leads to a synergistic effect, facilitate the desorption of H_{ads} and generation of H_2. (3). Based on the XRD (Fig. 3) and TEM (Fig. 2d) results, this amorphous structure is another reason for the excellent performance of PdCuNi-S catalyst. The lack of the long-range
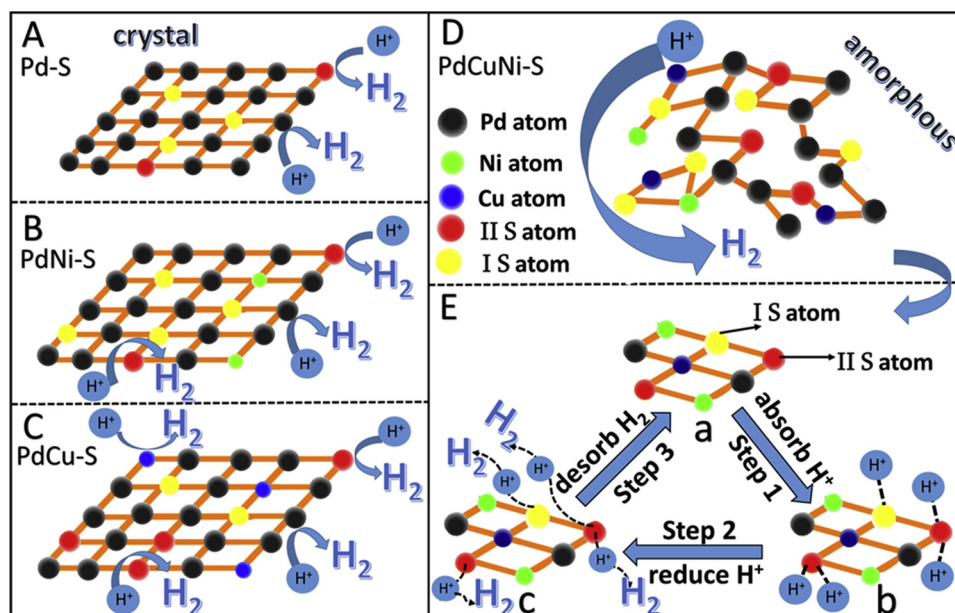

Fig. 8. Schematic diagram illustrating the hydrogen evolution mechanism: (A). Pd-S catalyst, (B). PdNi-S catalyst, (C). PdCu-S catalyst, (D). amorphous PdCuNi-S catalyst, and (E) the microstructure change of different S atoms in amorphous PdCuNi-S (D) during the hydrogen evolution.

ordered structure provides plenty of defect sites to act as active centers during the HER process. Compared with the widely research, the active sites of crystalline metarials, like the catalysts Pd-S、PdNi-S and PdCu-S in our experiment, only exists on the edges or surface. One of the most obvious advantages is that the whole amorphous PdCuNi-S catalyst (as shown in Fig. 8D) could function as the effective hydrogen evolution active center to promote the interfacial catalytic reactions. (4). According to most of reported [54] resules about amorphous sulfide materials, it is believed that the different S atoms have different catalytic effects on hydrogen evolution. On the basis of the similar mechanism, the introduction of element S in this work, especially the formation of the II S atoms (the higher binding energy bridging S_2^{2-} and/or apical S^{2-}), improved the intrinsic catalytic activity. To further explain the possible microstructure change of the different S atoms in amorphous PdCuNi-S during the hydrogen evolution, a schematic illustration is shown in Fig. 8E. Obviously, the different S atoms (Fig. 8E-a) show different H^+ adsorption ability during the reaction system. The II S atoms could capture two H^+ ions, while the I S atoms could only adsorb one H^+ ion because of their two-coordination structure (Fig. 8E-b). And subsequently, the adsorbed H^+ ions on the II S active sites could rapidly be reduced to release H_2 (Fig. 8E-c). Anyway, according to the above XPS analysis (Fig. 6 and Table S5), owing to the synergistic effects of Pd、Cu、Ni and S atoms during hydrogen evolution, the amorphous nanoporous PdCuNi-S catalyst show a excellent and stable hydrogen evolution performance.

4. Conclusions

In summary, we have successfully synthesized an amorphous nanoporous PdCuNi-S electrocatalyst via two-step dealloying method. The as-prepared PdCuNi-S catalyst exhibits excellent HER catalytic activity, which is very close to the commercial Pt/C in acid solution. The PdCuNi-S catalyst displays a small overpotential of 48 mV at 10 mA cm^{-2}, a low Tafel slope of 35 mV dec^{-1} and a high exchange current density of 385.45 μA cm^{-2}. The PdCuNi-S catalyst also exhibits good long-term stability for HER in acid solution. The bicontinuous nanoporous morphology, amorphous phase, improved charge transfer, more bridging S_2^{2-} and/or apical S^{2-} and synergetic effect of Pd, Cu, Ni and S are regarded as the reasons for the outstanding catalytic activity of PdCuNi-S catalyst. The amorphous PdCuNi-S electrocatalyst has huge application potential as a cost-effective non-Pt catalyst for water splitting.

Acknowledgements

Appendix A. Supplementary data

Supplementary material related to this article can be found, in the online version, at doi:https://doi.org/10.1016/j.apcatb.2019.01.030.

References

[1] P. Jiang, Q. Liu, X. Sun, NiP$_2$ nanosheet arrays supported on carbon cloth: an efficient 3D hydrogen evolution cathode in both acidic and alkaline solutions, Nanoscale 6 (2014) 13440–13445.

[2] Y. Hou, Z. Wen, S. Cui, S. Ci, S. Mao, J. Chen, An advanced nitrogen-doped graphene/cobalt-embedded porous carbon polyhedron hybrid for efficient catalysis of oxygen reduction and water splitting, Adv. Funct. Mater. 25 (2015) 872–882.

[3] X. Fan, Z. Peng, R. Ye, H. Zhou, X. Guo, M$_3$C (M: Fe, Co, Ni) nanocrystals encased in graphene nanoribbons: an active and stable bifunctional Electrocatalyst for oxygen reduction and hydrogen evolution reactions, ACS Nano 9 (2015) 7407–7418.

[4] W. Zhou, J. Zhou, Y. Zhou, J. Lu, K. Zhou, L. Yang, Z. Tang, L. Li, S. Chen, N-doped carbon-wrapped cobalt nanoparticles on n-doped graphene nanosheets for high-efficiency hydrogen production, Chem. Mater. 27 (2015) 2026–2032.

[5] L. Álvarez, G. Berhault, G. Alonso-Nuñez, Unsupported NiMo sulfide catalysts obtained from nickel/ammonium and nickel/tetraalkylammonium thiomolybdates: synthesis and application in the hydrodesulfurization of dibenzothiophene, Catal. Lett. 125 (2008) 35–45.

[6] F.H. Saadi, A.I. Carim, J.M. Velazquez, J.H. Baricuatro, C.C.L. McCrory, M.P. Soriaga, N.S. Lewis, Operando synthesis of macroporous molybdenum diselenide films for electrocatalysis of the hydrogen-evolution reaction, ACS Catal. 4 (2015) 2866–2873.

[7] D. Merki, S. Fierro, H. Vrubel, X. Hu, Amorphous molybdenum sulfide films as catalysts for electrochemical hydrogen production in water, Chem. Sci. 2 (2011) 1262–1267.

[8] A.B. Laursen, P.C. Vesborg, I. Chorkendorff, A high-porosity carbon molybdenum sulphide composite with enhanced electrochemical hydrogen evolution and stability, Chem. Commun. (Camb.) 49 (2013) 4965–4967.

[9] J. Tang, X. Zhao, Y. Zuo, P. Ju, Y. Tang, Electrodeposited Pd-Ni-Mo film as a cathode material for hydrogen evolution reaction, Electrochim. Acta 174 (2015) 1041–1049.

[10] Y. Song, X. Zhang, S. Yang, X. Wei, Z. Sun, Electrocatalytic performance for methanol oxidation on nanoporous Pd/NiO composites prepared by one-step dealloying, Fuel 181 (2016) 269–276.

[11] Z. Niu, Q. Peng, M. Gong, H. Rong, Y. Li, Oleylamine-mediated shape evolution of palladium nanocrystals, Angew. Chem. Int. Ed. Engl. 50 (2011) 6315–6319.

[12] J.W. Xiao, S.X. Fan, F. Wang, L.D. Sun, X.Y. Zheng, C.H. Yan, Porous Pd nanoparticles with high photothermal conversion efficiency for efficient ablation of cancer cells, Nanoscale 6 (2014) 4345–4351.

[13] J.M. Yang, S.A. Wang, C.L. Sun, M.D. Ger, Synthesis of size-selected Pt nanoparticles supported on sulfonated graphene with polyvinyl alcohol for methanol oxidation in alkaline solutions, J. Power Sources 254 (2014) 298–305.

[14] Y. Li, S. Chen, R. Long, H. Ju, Z. Wang, X. Yu, F. Gao, Z. Cai, C. Wang, Q. Xu, Near-surface dilution of trace Pd atoms to facilitate Pd-H bond cleavage for giant enhancement of electrocatalytic hydrogen evolution, Nano Energy 34 (2017) 306–312.

[15] L. Jing, L. Feng, S.X. Guo, Z. Jie, J. Ma, PdCu@Pd nanocube with Pt-like activity for hydrogen evolution reaction, ACS Appl. Mater. Inter. 9 (2017) 8151–8160.

[16] W. Xu, S. Zhu, Y. Liang, Z. Cui, X. Yang, A. Inoue, H. Wang, A highly efficient electrocatalyst based on amorphous Pd–Cu–S material for hydrogen evolution reaction, J. Mater. Chem. A Mater. Energy Sustain. 5 (2017) 35–42.

[17] R. Jana, A. Bhim, P. Bothra, S.K. Pati, S.C. Peter, Electrochemical dealloying of PdCu$_3$ nanoparticles to achieve Pt-like activity for the hydrogen evolution reaction, Chemsuschem 9 (2016) 2922–2927.

[18] F.A. Al-Odail, A. Anastasopoulos, B.E. Hayden, Hydrogen evolution and hydrogen oxidation on palladium bismuth alloys, Top. Catal. 54 (2011) 77–82.

[19] L. Chen, H. Guo, T. Fujita, A. Hirata, W. Zhang, A. Inoue, M. Chen, Nanoporous PdNi bimetallic catalyst with enhanced electrocatalytic performances for electro-oxidation and oxygen reduction reactions, Adv. Funct. Mater. 21 (2011) 4364–4370.

[20] X. Cao, Y. Han, C. Gao, Y. Xu, X. Huang, M. Willander, N. Wang, Highly catalytic active PtNiCu nanochains for hydrogen evolution reaction, Nano Energy 9 (2014) 301–308.

[21] X.C. Duan, H Nanoporous PdZr surface alloy as highly active non–platinum electrocatalyst toward oxygen reduction reaction with unique structure stability and methanol–tolerance, J. Power Sources 316 (2016) 106–113.

[22] B. Han, C. Xu, Nanoporous PdFe alloy as highly active and durable electrocatalyst for oxygen reduction reaction, Int. J. Hydrogen Energy 39 (2014) 18247–18255.

[23] W. Xu, S. Zhu, Y. Liang, Z. Li, Z. Cui, X. Yang, A. Inoue, Nanoporous CuS with excellent photocatalytic property, Sci. Rep. 5 (2015) 18125–18135.

[24] H. Ren, W. Xu, S. Zhu, Z. Cui, X. Yang, A. Inoue, Synthesis and properties of nanoporous Ag$_2$S/CuS catalyst for hydrogen evolution reaction, Electrochim. Acta 190 (2016) 221–228.

[25] H. Duan, Q. Hao, C. Xu, Nanoporous PtFe alloys as highly active and durable electrocatalysts for oxygen reduction reaction, J. Power Sources 269 (2014) 589–596.

[26] J. Sun, X. Yan, B. Zhao, L. Liu, Y. Gao, Z. Zhang, Modulation of compositions and electrocatalytic activities of quaternary nanoporous Pt-based alloys via controllable dealloying, Int. J. Hydrogen Energy 41 (2016) 9476–9489.

[27] X. Song, J. Hu, H. Zeng, Two-dimensional semiconductors: recent progress and future perspectives, J. Mater. Chem. C 1 (2013) 2952–2969.

[28] J. Wang, Z. Wang, D. Zhao, C. Xu, Facile fabrication of nanoporous PdFe alloy for nonenzymatic electrochemical sensing of hydrogen peroxide and glucose, Anal. Chim. Acta 832 (2014) 34–43.

[29] H.J. Lee, K.W. Kwon, C. Ryu, R. Sinclair, Thermal stability of a Cu/Ta multilayer: an intriguing interfacial reaction, Acta Mater. 47 (1999) 3965–3975.

[30] B.X. Liu, W.S. Lai, Q. Zhang, Irradiation induced amorphization in metallic multilayers and calculation of glass-forming ability from atomistic potential in the binary metal systems, Mater. Sci. Eng. R 29 (2000) 1–48.

[31] I.U.H. Toor, J. Ahmed, M.A. Hussein, F. Patel, N. Al-Aqeeli, Phase evolution studies during mechanical alloying of Fe$_{(82-x)}$-Cr$_{18}$-Si$_x$(x = 0, 1, 2, 3) alloy, J. Alloys. Compd. 683 (2016) 463–469.

[32] Z.J. Lin, M.J. Zhuo, Z.Q. Sun, P. Veyssière, Y.C. Zhou, Amorphization by dislocation accumulation in shear bands, Acta Mater. 57 (2009) 2851–2857.

[33] F. Xu, Y. Du, P. Gao, Z. Han, G. Chen, S. Wang, J. Jiang, Crystallization of melt-spun

Mg₆₃Ni₂₂Pr₁₅ amorphous alloy ribbon, J. Alloys. Compd. 441 (2007) 76–80.

[34] F. Scaglione, P. Rizzi, F. Celegato, L. Battezzati, Synthesis of nanoporous gold by free corrosion of an amorphous precursor, J. Alloys. Compd. 615 (2014) S142–S147.

[35] K. Kwon, H. Lee, R. Sinclair, Solid-state amorphization at tetragonal-Ta/Cu interfaces, Appl. Phys. Lett. 75 (1999) 935–937.

[36] A. Inoue, Stabilization of metallic supercooled liquid and bulk amorphous alloys, Acta Mater. 48 (2000) 279–306.

[37] A. Takeuchi, A. Inoue, Calculations of mixing enthalpy and mismatch entropy for ternary amorphous alloys, Mater. T. Jim. 41 (2000) 1372–1378.

[38] L. Yang, X. Wu, X. Zhu, C. He, M. Meng, Z. Gan, P.K. Chu, Amorphous nickel/cobalt tungsten sulfide electrocatalysts for high-efficiency hydrogen evolution reaction, Appl. Surf. Sci. 341 (2015) 149–156.

[39] K.C. Pham, Y.H. Chang, D. McPhail, C. Mattevi, A.T. Wee, D.H. Chua, Amorphous molybdenum sulfide on graphene-carbon nanotube hybrids as highly active hydrogen evolution reaction catalysts, ACS Appl. Mater. Inter. 8 (2016) 5961–5971.

[40] B.B. Li, S.Z. Qiao, X.R. Zheng, X.J. Yang, Z.D. Cui, S.L. Zhu, Z.Y. Li, Y.Q. Liang, Pd coated MoS₂ nanoflowers for highly efficient hydrogen evolution reaction under irradiation, J. Power Sources 284 (2015) 68–76.

[41] S. Gupta, N. Patel, R. Fernandes, R. Kadrekar, A. Dashora, A.K. Yadav, D. Bhattacharyya, S.N. Jha, A. Miotello, D.C. Kothari, Co–Ni–B nanocatalyst for efficient hydrogen evolution reaction in wide pH range, Appl. Catal. B: Environ 192 (2016) 126–133.

[42] Y.H. Chang, C.T. Lin, T.Y. Chen, C.L. Hsu, Y.H. Lee, W. Zhang, K.H. Wei, L.J. Li, Highly efficient electrocatalytic hydrogen production by MoS(x) grown on graphene-protected 3D Ni foams, Adv. Mater. 25 (2013) 756–760.

[43] S. Tang, B. Zhu, X. Shi, J. Wu, X. Meng, General controlled sulfidation toward achieving novel nanosheet-built porous square-FeCo₂S₄-tube arrays for high-performance asymmetric all-solid-state pseudocapacitors, Adv. Energy Mater. 7 (2017) 1601985–1601995.

[44] L.R.L. Ting, Y. Deng, L. Ma, Y.J. Zhang, A.A. Peterson, B.S. Yeo, Catalytic activities of sulfur atoms in amorphous molybdenum sulfide for the electrochemical hydrogen evolution reaction, ACS Catal. 6 (2016) 861–867.

[45] T. Hengsawad, T. Jindarat, D.E. Resasco, Synergistic effect of oxygen vacancies and highly dispersed Pd nanoparticles over Pd-loaded TiO₂ prepared by a single-step sol–gel process for deoxygenation of triglycerides, Appl. Catal. A Gen. 566 (2018) 74–86.

[46] B. Zhang, X. Zheng, O. Voznyy, R. Comin, M. Bajdich, M. García-Melchor, L. Han, J. Xu, M. Liu, L. Zheng, Homogeneously dispersed multimetal oxygen-evolving catalysts, Science 352 (2016) 333–337.

[47] S. Chu, W. Chen, G. Chen, J. Huang, R. Zhang, C. Song, X. Wang, C. Li, K.K. Ostrikov, Holey Ni-Cu phosphide nanosheets as a highly efficient and stable electrocatalyst for hydrogen evolution, Appl. Catal. B: Environ. 243 (2019) 537–545.

[48] V.R. Stamenkovic, B. Fowler, B.S. Mun, G. Wang, P.N. Ross, A.L. Christopher, M.M. Nenad, Improved oxygen reduction activity on Pt₃Ni(111) via increased surface site availability, Science 315 (2007) 493–497.

[49] D.Y. Wang, M. Gong, H.L. Chou, C.J. Pan, H.A. Chen, Y. Wu, M.C. Lin, M. Guan, J. Yang, C.W. Chen, Highly active and stable hybrid catalyst of cobalt-doped FeS₂ nanosheets-carbon nanotubes for hydrogen evolution reaction, J. Am. Chem. Soc. 137 (2015) 1587–1592.

[50] T. Chao, X. Luo, W. Chen, B. Jiang, J. Ge, Y. Lin, G. Wu, X. Wang, Y. Hu, Z. Zhuang, Atomically dispersed copper–platinum dual sites alloyed with palladium nanorings catalyze the hydrogen evolution reaction, Angew. Chem. 129 (2017) 16047–16051.

[51] M. Gong, W. Zhou, M.C. Tsai, J. Zhou, M. Guan, M.C. Lin, B. Zhang, Y. Hu, D.Y. Wang, J. Yang, Nanoscale nickel oxide/nickel heterostructures for active hydrogen evolution electrocatalysis, Nat. Commun. 5 (2013) 4695–4700.

[52] Y. Li, H. Wang, L. Xie, Y. Liang, G. Hong, H. Dai, MoS₂ nanoparticles grown on graphene: an advanced catalyst for the hydrogen evolution reaction, J. Am. Chem. Soc. 133 (2011) 7296–7299.

[53] D. Merki, X. Hu, Recent developments of molybdenum and tungsten sulfides as hydrogen evolution catalysts, Energy Environ. Sci. 4 (2011) 3878–3888.

[54] H. Yu, P. Xiao, P. Wang, J. Yu, Amorphous molybdenum sulfide as highly efficient electron-cocatalyst for enhanced photocatalytic H₂ evolution, Appl. Catal. B: Environ. 193 (2016) 217–225.

[55] D. Jie, W. Qiang, H. Cunping, Y. Weifeng, X. Qunjie, Cost effective Mo rich Mo₂C electrocatalysts for hydrogen evolution reaction, J. Mater. Chem. A 10028 (2018) 10028–10035.

[56] J. Kubisztal, A. Budniok, A. Lasia, Study of the hydrogen evolution reaction on nickel-based composite coatings containing molybdenum powder, Int. J. Hydrogen Energy 32 (2007) 1211–1218.

[57] J. Chen, J. Wang, J. Chen, L. Wang, A bifunctional electrocatalyst of PtNi nanoparticles immobilized on three-dimensional carbon nanofiber mats for efficient and stable water splitting in both acid and basic media, J. Mater. Sci. 52 (2017) 13064–13077.

[58] R. Solmaz, K. Gülfeza, Electrochemical deposition and characterization of NiFe coatings as electrocatalytic materials for alkaline water electrolysis, Electrochim. Acta 54 (2009) 3726–3734.

[59] Y. Tan, H. Wang, P. Liu, Y. Shen, C. Cheng, A. Hirata, T. Fujita, Z. Tang, M. Chen, Versatile nanoporous bimetallic phosphides towards electrochemical water splitting, Energy Environ. Sci. 9 (2016) 2257–2261.

[60] K. Xiong, L. Li, L. Zhang, W. Ding, L. Peng, Y. Wang, S. Chen, S. Tan, Z. Wei, Ni-doped MoC nanowires supported on Ni foam as a binder-free electrode for enhancing the hydrogen evolution performance, J. Mater. Chem. A 3 (2015) 1863–1867.

[61] D. Kong, J.J. Cha, H. Wang, H.R. Lee, Y. Cui, First-row transition metal dichalcogenide catalysts for hydrogen evolution reaction, Energy Environ. Sci. 6 (2013) 3553–3558.